Signatures of Induced Vertical Air Motion Accompanying Quasi-Horizontal Roll-Up of Stratospheric Intrusions

VOLKMAR WIRTH

Meteorologisches Institut, Universität München, Munich, Germany

CHRISTOF APPENZELLER*

Department of Atmospheric Sciences, University of Washington, Seattle, Washington

MARTIN JUCKES

Meteorologisches Institut, Universität München, Munich, Germany

(Manuscript received 24 July 1996, in final form 5 February 1997)

ABSTRACT

The quasi-horizontal roll-up of unstable stratospheric intrusions into isolated vortices is known to result in specific structures on satellite water vapor images that are characterized by intermingling dark and light filaments. The current paper investigates how these features are generated and how they relate to partly similar features found on concurrent maps of the tropopause height or potential vorticity (PV). The roll-up of a stratospheric intrusion is simulated numerically with an idealized quasigeostrophic model, which focuses on the dynamics induced by anomalies in the height of the tropopause. The upper-tropospheric adiabatic vertical wind is calculated explicitly and is used to simulate water vapor images in the model. These images show qualitatively the same characteristic features as observed. They are generated through a combination of horizontal advection of initial moisture anomalies and the creation of additional moisture anomalies resulting from the upper-tropospheric vertical air motion. The latter is, in turn, induced by the quasi-horizontal motion of the tropopause anomaly. It is suggested that a substantial portion of the spiral-like structures on the water vapor images is likely to reflect the vertical wind induced by the evolution of the intrusion itself. When the tropopause is defined through a fairly low value of PV, it may acquire similar spiraling structures, as it is being advected almost like a passive tracer. On the other hand, for the dynamically active core part of the intrusion, which is located at higher values of PV, one may expect an evolution leading to more compact vortex cores and less structure overall.

1. Introduction

Water vapor (WV) images from satellites probing the midlatitude upper troposphere often display complex structures on synoptic and subsynoptic scales. Broadly speaking, regions of low humidity at upper-tropospheric heights appear as regions of high radiance typically displayed with dark shading, while moist and cloudy regions have low radiance, displayed with light shading. Manney and Stanford (1987) suggested that under certain assumptions there should be a correspondence between the structures on WV images and on isentropic maps of potential vorticity (PV) in the upper troposphere, although they were able to find only a qualitative relationship between the two datasets. Nevertheless, at least in the case of a deep intrusion of stratospheric air into the troposphere, one may expect a good correlation, as stratospheric air is distinguished from tropospheric air by low concentrations of WV and high values of PV.

Through juxtaposition of *Meteosat-4* WV images with European Centre for Medium-Range Weather Forecasts (ECMWF) isentropic maps of PV, Appenzeller and Davies (1992) showed that stratospheric intrusions can develop into elongated streamers of stratospheric air and subsequently break and roll up into several subvortices. Due to the limited spatial resolution of the ECMWF analyses, these maps could not possibly render as much detail in the finescale structure as seen on the high-resolution water vapor images. To overcome this limitation, Appenzeller et al. (1996) applied a contour advection technique (CAT) to contours of PV on isentropic surfaces using winds from ECMWF analyses. They showed that the instability-like fragmentation has the potential to create rich subsynoptic to mesoscale struc-

* Current affiliation: Climate and Environmental Physics, University of Bern, Bern, Switzerland.

Corresponding author address: V. Wirth, Meteorologisches Institut, Theresienstraß 37, 80333 München, Germany.
E-mail: volkmar@werner.meteo.physik.uni-muenchen.de

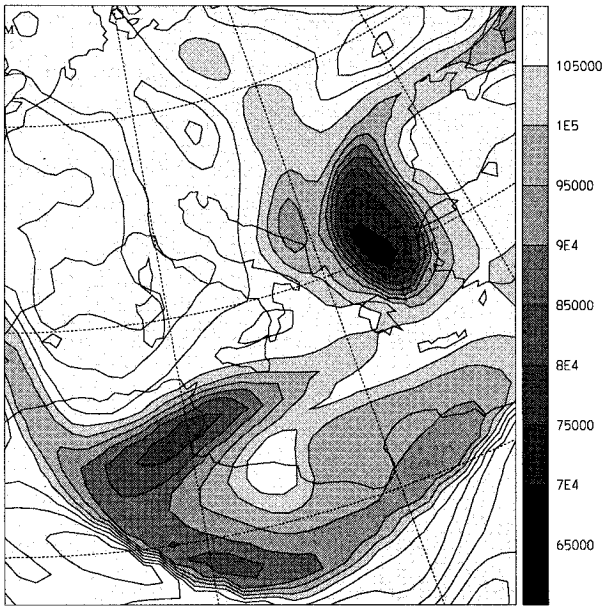

FIG. 1. Geopotential ($m^2\ s^{-2}$) at the tropopause over Europe at 0000 UTC 14 May 1992. The tropopause is defined as the surface on which PV = 2 PVU. Calculations are based on ECMWF T213/31 initialized analysis data. The contours are every $5 \times 10^3\ m^2\ s^{-2}$, and heights below $1.05 \times 10^5\ m^2\ s^{-2}$ are shaded. The height of the tropopause can be obtained by dividing the contoured values by the gravity acceleration.

tures near the tropopause with intermingling spiral-like filaments of low PV tropospheric and high PV stratospheric air. The agreement in some of their CAT calculations with the observed WV images was remarkable. In others, their calculations were at variance with the observations. Since the WV channel does not actually measure PV on an isentrope, this partial disagreement is not too surprising. In a case study of another fragmenting PV strip, Browning (1993) argued that one has to account for the effect of the upper tropospheric vertical wind on the moisture distribution in order to fully explain the observed moisture and cloud features on the satellite images.

In the current paper we want to investigate the following question: How, in the context of the quasi-horizontal roll-up of a fragmenting stratospheric intrusion, are the small-scale structures on WV satellite images generated, and how are they related to the structure of the tropopause? To this end, we will explicitly keep track of upper-tropospheric vertical air motions and their impact on the formation of radiance anomalies in the WV images. We assume that the relevant vertical wind is, to a first approximation, the ageostrophic wind induced by the quasi-balanced horizontal motion of the stratospheric intrusion itself. Although the upper-tropospheric air motion is related to the motion of the tropopause anomaly, the former is not necessarily parallel to the latter and the structures developing on the water vapor image need not be identical to the structures of the intrusion.

To investigate these ideas, we use an idealized model of quasigeostrophic tropopause (QGT) dynamics in which the tropopause is idealized as a steplike transition between a low-PV troposphere and a high-PV stratosphere. By construction, this model focuses on dynamical processes that are dominated by the tropopause anomaly alone. A more complex evolution requiring the interaction between features in the upper and lower troposphere (Hoskins et al. 1985; Browning and Roberts 1994, 1995) is excluded from the current considerations. In addition to modeling the evolution of the tropopause, we will simulate WV images. This will allow us to compare model-generated WV images with the model tropopause on the one hand and with real WV images on the other hand.

The paper is organized as follows. In section 2 we review the tropopause structure and WV satellite images for the case of an observed fragmenting intrusion. Section 3 describes the model. Model runs and their interpretation are then presented in section 4, where we develop a simplified picture of how WV images are formed, compare our model runs with actual Meteosat WV images, and discuss the different degrees of structure seen on the different maps. Finally, a summary and conclusions are provided in section 5.

2. Observations

a. The tropopause structure on ECMWF analyses

Figure 1 shows the observed geopotential at the dynamically defined tropopause [PV = 2 PVU, with 1 PVU = 10^{-6} K $m^2\ kg^{-1}\ s^{-1}$; see Hoskins et al. (1985)] for a fragmenting stratospheric intrusion that developed on 14 May 1992 over Europe. A detailed description of this case was given in Appenzeller et al. (1996). The calculations were done using ECMWF T213/31 initialized analyses. These data represent a blend of operational observations with the model's own 6-h forecast; in midlatitude they have a resolution of about 60 km × 60 km × 2 km. The instability-like fragmentation of the initially elongated stratospheric intrusion led to the development of two distinct subvortices: one was over northern Greece and a second was over Tunisia. In the coarse-grained ECMWF data the vortex over Greece appears as a relative circular anomaly. The vortex over Tunisia started to develop 12 h later and revealed a more anchor-shaped pattern. In both vortices the tropopause was substantially displaced downward with a maximum displacement of approximately 3–4 km relative to the surrounding tropopause. The potential temperature anomaly was of the order of 15 K.

b. Water vapor satellite images

The corresponding WV satellite image shown in Fig. 2a is taken from the European satellite *Meteosat-4*. The

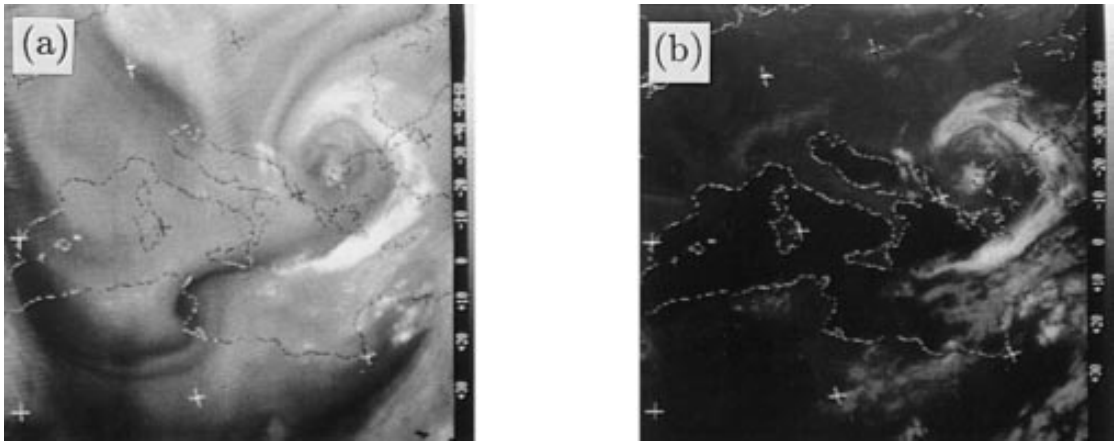

FIG. 2. Same case as in Fig. 1: (a) *Meteosat-4* water vapor satellite image, 1200 UTC 14 May 1992. A dark region signifies high radiance values and indicates anomalously low humidity at upper-tropospheric altitudes. (b) *Meteosat-4* infrared cloud image, 1230 UTC 14 May 1992. A white region signifies low temperatures indicating high clouds.

spectral region of the WV channel is centered within the 6.3-μm water vapor absorption band (1342–1174 cm^{-1}). Its images have a horizontal resolution of about 8 km $\times$ 5 km in midlatitudes, and the display is graduated in 256 gray levels such that the darker the shading, the higher the radiance values (Honvault 1990). High clouds are characterized by low radiance values and typically appear as white areas. Radiative transfer calculations for a cloud-free atmosphere (Poc et al. 1980; Fischer et al. 1981) indicate that the weighting and contribution function profiles typically peak between 7 and 9 km, and the radiance measured is primarily sensitive to the amount of water vapor above the 600-hPa level.

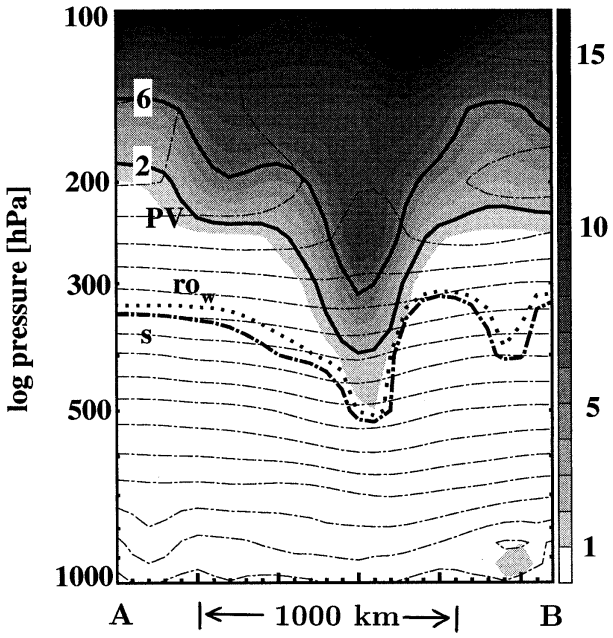

FIG. 3. Vertical cross section through the stratospheric intrusion at 0000 UTC 13 May 1992. Time and location as in Figs. 11c and 11d in Appenzeller et al. (1996), i.e., going from point A (48°N, 12°E) to point B (39.7°N, 30.5°E) with ticks every 63 km. The shaded area represents PV larger than 1 PVU. Also shown are the temperature distribution (thin dashed contours every 5 K, starting at the ground with 285 K), the dynamical tropopause defined as a PV = 2 PVU surface (thick solid line), a water vapor density surface with ρ_w = 75 mg m^{-3} (dotted line), and a specific humidity surface with s = 177 mg kg^{-1} (thicker dash–dotted line).

Figure 3 shows a vertical cross section through the stratospheric intrusion discussed above. The origin of these data are, again, ECMWF analyses [see Appenzeller et al. (1996), for details; as for time and location, our Fig. 3 corresponds to the vertical cross sections shown in their Figs. 11c and 11d]. Stratospheric air characterized by high PV is shaded, and the dynamical tropopause (i.e., the 2-PVU line) is marked by a thick line. The shaded region is also characterized by low humidity. In the vertical section, the stratospheric streamer appears as a dry zone penetrating deeply into the upper troposphere from above. This dry region appears as a dark band of high radiance values in the WV satellite image.

Prior to the fragmentation, on the WV images, a ''dark'' band of high radiance was stretching southwestward over eastern and southern Europe. On 14 May, the WV satellite images clearly reveal the complicated, highly nonlinear evolution following the fragmentation process (Fig. 2a). They showed a spiral-like structure of high and low radiance within the region of the vortex located over Greece and dark filaments of high radiance in between and outside the vortices. The pattern in the other vortex over Tunisia suggested that its roll-up process was still in an early stage. Indications of the vortex roll-up were also found in the *Meteosat-4* infrared satellite images (Fig. 2b), where a swirling comma of high clouds developed together with a cloudy patch in the center of the vortex over Greece.

The finescale structures on the WV images are not resolved on the ECMWF tropopause potential temper-

ature map or isentropic PV map (cf. Fig. 1). However, a comparatively rich Lagrangian vortical structure at the lower edge of the stratospheric streamer can be ''observed'' when a CAT is used to dramatically increase the data resolution (see Plate 2 in Appenzeller et al. 1996). For the later discussion, two features concerning the finescale structure in these CAT calculations appear noteworthy. First, the connecting filaments, albeit present, are much thinner in the CAT calculation than the corresponding features on the WV images. Second, throughout the roll-up process, the CAT calculations are generally characterized by dark values (i.e., high PV) in the vortex center, while in the WV image in the current example, on the other hand, the initially dry feature in the vortex center is replaced by a white (moist) feature during the roll-up process. Both points will be specifically addressed below in the discussion of our model-generated WV images.

One can express the radiance R received by the WV channel of a satellite in terms of the ''equivalent blackbody temperature'' $T_{\rm bb}$ as follows:

$$R = \int_0^\infty B_\nu(T_{\rm bb})\omega(\nu)\, d\nu, \tag{1}$$

where ν is the frequency, $\omega(\nu)$ is the WV channel spectral response function, and $B_\nu(T)$ is the Planck function for temperature T. Simplified theoretical considerations indicate that in a cloud-free atmosphere the equivalent blackbody temperature $T_{\rm bb}$ is equal to the temperature of the atmosphere at the peak of the weighting function. The latter, in turn, is approximately located on an isosteric surface, that is, a surface of constant water vapor density ρ_w (Ramond et al. 1981), namely, $\rho_w = 75 \times 10^{-6}$ kg m^{-3} (see the dotted line in Fig. 3). The location of this isosteric surface will be called the ''effective level of emission.'' Except in the east (right-hand side) of the vertical section in Fig. 3, the effective level of emission follows roughly the displacement of the tropopause but is displaced downward by 1–2 km. The thick dash–dotted line represents a surface of constant specific humidity $s = \rho_w/\rho = 177$ mg kg^{-1} (where ρ denotes the density of air). Its vertical displacement is almost parallel to the displacement of the isosteric surface. This indicates that the vertical displacement of the specific humidity surface gives a good approximation for the location of the effective level of emission.

For the case of a vertically oriented stratospheric intrusion, the approximations suggested by Ramond et al. (1981) have been confirmed for instance by the calculations of Appenzeller et al. (1996). They showed that the temperature field on a specific isosteric surface in the ECMWF model has structures that are qualitatively very similar to the structures on the corresponding WV image, except for the lower resolution of the model-generated map. Thus, the above provides a physically meaningful interpretation of the measured radiance field and will be used in the following as a basis for simulating WV images in the model.

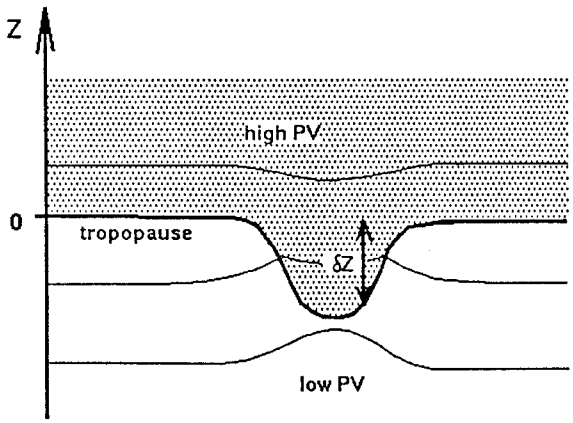

FIG. 4. Schematic representation of the model showing a vertical section through a stratospheric intrusion. The heavy line is the tropopause, while the thin solid lines delineate isentropes. A downward displaced tropopause corresponds to a colder than normal tropopause according to Eq. (2).

3. The model

a. General features and model equations

The model used in the current study has been suggested by Juckes (1994) for the study of QGT dynamics. The tropopause is idealized as the interface between two volumes of homogeneous quasigeostrophic PV, with one value in the troposphere and a higher value in the stratosphere (Fig. 4). The tropopause is treated as a material surface that is allowed to be displaced by the amount δz from its unperturbed position. Neglecting effects from the lower boundary, Juckes shows that in the framework of quasigeostrophic theory on an f-plane with the Boussinesq approximation, the tropopause displacement δz from its unperturbed position ($z = 0$) is proportional to the potential temperature anomaly $\theta'_{\rm tp}$ at the tropopause,

$$\delta z(\mathbf{x}) = \frac{g\theta'_{\rm tp}(\mathbf{x})}{N_t N_s \theta_{\rm oo}}, \tag{2}$$

where $\mathbf{x} = (x, y)$ denotes the horizontal position, g is the gravity acceleration, $\theta_{\rm oo}$ is a reference value of the potential temperature, and N_t and N_s denote the Brunt–Väisälä frequency of the troposphere and stratosphere, respectively. With typical values for the different parameters, as given below, a tropopause temperature anomaly of 15 K corresponds to a downward displacement of the tropopause of about 2.5 km. This is somewhat less than the 3–4 km in the observed case from Fig. 1, but it is in fairly good agreement with larger-scale climatological data from an atmospheric GCM (Juckes 1994).

In this model, the troposphere extends to $z \to -\infty$ and the stratosphere to $z \to +\infty$. Potential vorticity

anomalies can only occur through displacements of the tropopause. For convenience, we first consider a single Fourier mode,

$$\theta'_{\rm tp}(\mathbf{x}) = \hat{\theta}_{\rm tp}(\mathbf{k}) \exp(i\mathbf{k}\cdot\mathbf{x}), \tag{3}$$

with the horizontal wave vector $\mathbf{k} = (k, l)$, where the real part is to be understood. A more general perturbation can be obtained by linear superposition. Matching of the solution at the displaced tropopause and requiring the solution to decay as $z \to \pm\infty$ leads to the following geostrophic streamfunction (seeJuckes 1994):

$$\psi(x, y, z) = \psi_o(\mathbf{k}) \exp(i\mathbf{k}\cdot\mathbf{x}) \exp\left(-\frac{N}{f}K|z|\right), \tag{4}$$

where $K = (k^2 + l^2)^{1/2}$, f is the (constant) Coriolis parameter,

$$\psi_o(\mathbf{k}) = \frac{g(N_s - N_t)}{\theta_{\rm oo}N_sN_t}\frac{\hat{\theta}_{\rm tp}(\mathbf{k})}{K}, \tag{5}$$

and

$$N = \begin{cases} N_s, & z > 0, \\ N_t, & z < 0. \end{cases} \tag{6}$$

The two components of the geostrophic wind $u_g(x, y, z)$ and $v_g(x, y, z)$, and the potential temperature perturbation $\theta'(x, y, z)$, are given by

$$(u_g, v_g) = \left(-\frac{\partial\psi}{\partial y}, \frac{\partial\psi}{\partial x}\right), \tag{7}$$

and

$$\theta' = \frac{f\theta_{\rm oo}}{g}\frac{\partial\psi}{\partial z}. \tag{8}$$

Note that, by construction, the anomaly θ' is discontinuous across $z = 0$, but that the total potential temperature is continuous across the displaced tropopause at $z = \delta z$.

Assuming material conservation of tropopause potential temperature,

$$\frac{D_g}{Dt}\theta'_{\rm tp}(x, y, t) \equiv \frac{\partial\theta'_{\rm tp}}{\partial t} + u_g\frac{\partial\theta'_{\rm tp}}{\partial x} + v_g\frac{\partial\theta'_{\rm tp}}{\partial y} = 0, \tag{9}$$

one obtains an equation for the evolution of $\theta'_{\rm tp}$. The wind at the tropopause (u_g, v_g) in Eq. (9) can be evaluated at $z = 0$ within the quasigeostrophic approximation. Equation (9), together with (3), (4), and (7) constitute a closed system of equations, which in combination with linear superposition allows us to calculate the time evolution of $\theta'_{\rm tp}(\mathbf{x}, t)$, $\delta z(\mathbf{x}, t)$, and $\psi(x, y, z, t)$ from any given initial tropopause displacement $\delta z(\mathbf{x}, t_0)$. The dynamics of this version of Juckes's model is equivalent to ''surface quasigeostrophic dynamics'' (Held et al. 1995); it differs in certain features from the more familiar barotropic vortex dynamics (Wirth 1996).

A key issue in the current investigation is the ageostrophic vertical wind w induced by the geostrophic flow. It is obtained for any $z \neq 0$ by solving

$$\frac{\partial\theta'}{\partial t} + u_g\frac{\partial\theta'}{\partial x} + v_g\frac{\partial\theta'}{\partial y} + w\frac{\partial\theta_o}{\partial z} = 0 \tag{10}$$

for w, where $\partial\theta_o/\partial z = g^{-1}N^2\theta_{\rm oo}$. Although in this formulation w is generally represented as a small residuum of several large terms, its calculation turns out to be numerically robust.

We also note that using the hydrostatic equation to relate δz to a tropopause pressure anomaly gives $p'_{\rm tp} = -g\rho_0\delta z$. Here, the pressure anomaly at $z = 0$, which is relatively small if $k \gg (N_s - N_t)f/g \approx 10^{-7}$ m^{-1}, has been neglected. The linearized equation of state reads

$$\frac{\theta'_{\rm tp}}{\theta_{\rm oo}} = \frac{T'_{\rm tp}}{T_o} - \kappa\frac{p'_{\rm tp}}{p_o}. \tag{11}$$

Equation (2) can then be converted into a relation between the temperature anomaly $T'_{\rm tp}$ and the potential temperature anomaly $\theta'_{\rm tp}$ or the tropopause displacement δz,

$$\frac{T'_{\rm tp}}{T_o} = \left(1 - \frac{g^2}{T_oc_pN_sN_t}\right)\frac{\theta'_{\rm tp}}{\theta_{\rm oo}} \approx -\frac{\theta'_{\rm tp}}{\theta_{\rm oo}} = -\frac{N_sN_t}{g}\delta z, \tag{12}$$

where the prime in connection with subscript tp denotes the anomaly of a quantity on the displaced tropopause relative to its unperturbed value at its unperturbed height. When, for instance, a cold cyclonic cutoff is formed, it is cold relative to unperturbed air at the same height, but the tropopause is lower and therefore warmer than its unperturbed state. With the further broad assumption that anomalies in the WV radiance represent tropopause temperature anomalies (cf. appendix A), Eq. (12) could be used to estimate δz from these radiances. One of the main aims of this paper is to show that the actual relationship is more complex, even within the idealized quasigeostrophic model.

b. Assumptions and limitations

Admittedly the model is rather idealized and cannot be used for a quantitatively correct simulation. It is considered here to yield a qualitative representation of the relevant upper-tropospheric dynamics. Two major assumptions have to be satisfied. First, the dynamics must be determined by anomalies of the tropopause itself rather than other features such as, for instance, temperature anomalies at the earth's surface. This assumption appears justified in the current context, as the stratospheric intrusions under consideration should be both strong enough and of small enough scale so that their dynamics will be determined by their own structure to a first approximation. The second major assumption is quasigeostrophy, which requires that

$$\delta z \ll LfN^{-1}, \tag{13}$$

where L is a characteristic horizontal length (Juckes

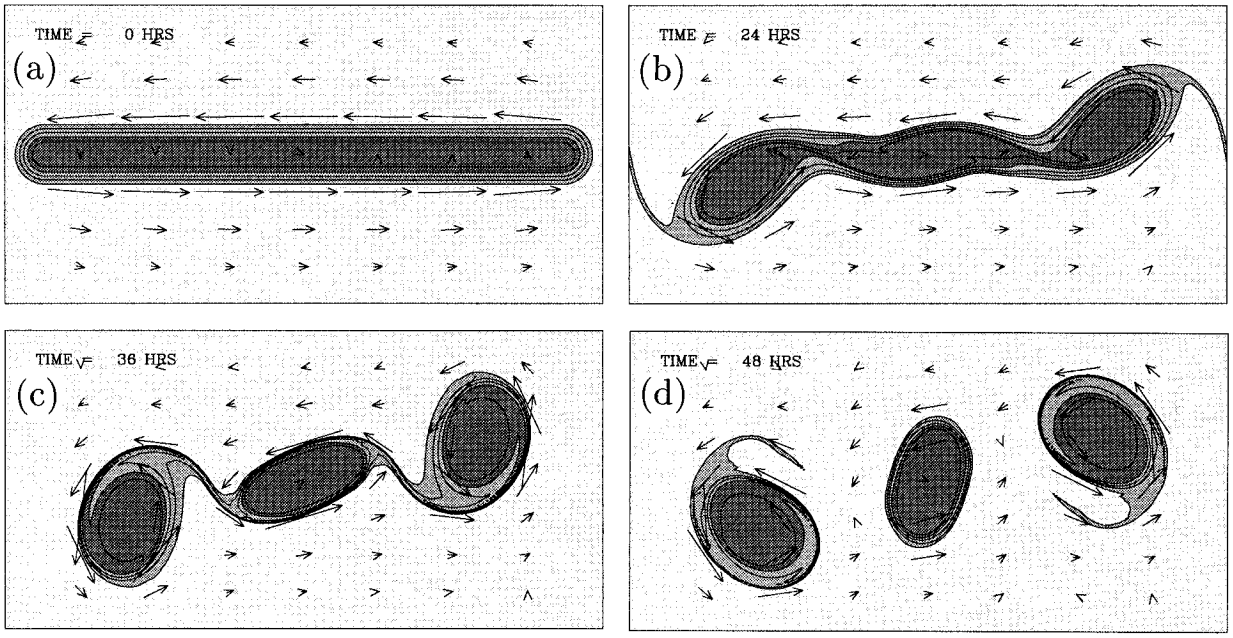

FIG. 5. Evolution of a stratospheric intrusion in the idealized model: (a) initial state, (b) after 24 h, (c) after 36 h, and (d) after 48 h. The contours delineate the downward tropopause displacement δz (the contour interval is 500 m, no zero contour), and the dark shading indicates relatively large downward displacement. The arrows represent the geostrophic wind at $z = 0$.

1994). The model describes the limit of very shallow intrusions of a sharp tropopause. Following Bretherton (1966), Juckes (1994) has shown that the potential temperature distribution on the vertically displaced tropopause is mathematically equivalent to an infinitely shallow quasigeostrophic PV distribution according to

$$q_g(x, y, z) = -\frac{fg}{\theta_{oo}}\left(\frac{N_s^2 - N_t^2}{N_s^2 N_t^2}\right)\theta'_{tp}(x, y)\delta(z) \quad (14)$$

in this limit. Through this result QGT dynamics can be interpreted as a model for the evolution of the vertically integrated PV. The latter has been used by Shapiro and Grell (1994) to visualize tropopause structures.

For the deep intrusions of small horizontal scales, which we investigate in this work, the assumptions concerning the shallowness of the intrusions are not satisfied, and the model cannot be used in quantitative terms. For instance, our experience with the QGT model suggests that the exponential decay with $|z|$ described by Eq. (4) overestimates the actual decay of a deep anomaly away from the tropopause. Yet even in situations where its approximating assumptions are violated, quasigeostrophic theory has often been regarded as a good qualitative guide. The same approach is adopted here, and we will interpret the model only in qualitative terms displaying the simulated WV images in the form of gray shadings. The fact that our simulated WV images resemble observed WV images in many aspects is taken as an a posteriori justification for the use of the model in the current context.

c. Numerics

The model equations are integrated numerically using a standard pseudospectral method with doubly periodic boundary conditions. The resolution corresponds to $M_x = 256$ and $M_y = 128$ wavenumbers in the zonal and meridional direction, respectively. Hyperviscosity is included for numerical stability by adding $\nu\nabla^6\theta'_{tp}$ on the right-hand side of Eq. (9) with the coefficient ν chosen so that the dissipation timescale at the largest retained wavenumber is ten time steps. For time stepping a second-order Adams–Bashforth scheme is used with explicit treatment of the hyperviscous term. The time step $\Delta t = 30$ s was chosen small enough so that computational stability is guaranteed throughout the integration. To diagnose $w(t)$ from Eq. (10), the time tendency $\partial\theta'(t)/\partial t$ is approximated by $[\theta(t) - \theta(t - \Delta t)]/\Delta t$. The experiments reported have domain size 1024 km $\times$ 2048 km. Other domain sizes have been tried, and the essential features of the results were unaltered. The remaining parameters have been chosen as in Juckes (1994): $f = 1 \times 10^{-4}$ s^{-1}, $g = 10$ m s^{-2}, $\theta_{oo} = 300$ K, $N_t = 10^{-2}$ s^{-1}, and $N_s = 2 \times 10^{-2}$ s^{-1}.

4. Model runs and their interpretation

The initial state for our model integration is given in Fig. 5a. It is assumed to represent a streamerlike stratospheric intrusion previously generated by quasi-horizontal advection from more poleward latitudes. Guided by cross sections such as the one shown in Fig. 3 (cf.

also Browning 1993; and Appenzeller et al. 1996), it is designed as a finite strip with a V-shaped profile in the vertical section. The length of the strip is about 2000 km, its full width at half maximum is 150 km, and its maximum intrusion is 2.8 km. The maximum geostrophic wind induced by this tropopause anomaly is 21 m s^{-1}. The dimensions have been chosen so as to represent a typical atmospheric scenario.

Figures 5b, 5c, and 5d show the state of the fragmenting intrusion after 24, 36, and 48 h of integration, respectively. The strip breaks up into three isolated vortices. The evolution has the character (inter alia vortex spacing) of the instability that would grow on an infinitely long strip (cf. Schär and Davies 1990) but is modified by the finite-amplitude effects at the ends of the strip. Furthermore, Fig. 5 clearly shows the well-known tendency of two-dimensional and geostrophic flows to concentrate PV in separate isolated vortices, which are almost axisymmetric and which have a rather uniform vortex core with sharp PV gradients at the vortex edge (McWilliams 1984; Melander et al. 1987; Legras and Dritchel 1993). The thin filaments connecting the three vortices are lost after 1.5–2 days owing to the model diffusion. The model evolution appears somewhat slow compared with typical real world cases; this is likely to be a particular feature of the QGT model that tends to underestimate the speed of the roll-up of deep intrusions as compared to the nondivergent barotropic model (Wirth 1996). In the following, maps of the tropopause anomaly as in Fig. 5 will simply be referred to as ''tropopause maps.'' Recall, however, that in the framework of our QGT model they can just as well be interpreted as maps of the temperature anomaly on the displaced tropopause [Eq. (2)] or as maps of a vertically integrated PV anomaly [Eq. (14)]. The question of how the tropopause in our simple model relates to the tropopause in more realistic models or in the real atmosphere will be addressed in more detail in section 4d.

A downward displacement of the tropopause corresponds to an intrusion of dry stratospheric air into the troposphere, which presumably results in a dark area on the WV satellite image (see end of section 3a). To simulate this effect, the intensity of the shading in Fig. 5 increases with increasing depth δz of the stratospheric intrusion. To a first approximation, the vortex roll-up in Fig. 5 resembles the behavior that is often observed on WV satellite images. However, on actual WV images there appears to be more detailed structure with spiraling dark and light filaments and sometimes with white patches right in the center of the vortex (Fig. 2a). Despite the high horizontal resolution of the model, these features are not seen in Fig. 5, where the filaments are very weak and where the vortex center is uniform and dark (see also Schär and Davies 1990; Held et al. 1995; Juckes 1995)

As discussed earlier, the WV channel radiance is not really determined by the displacement of the tropopause

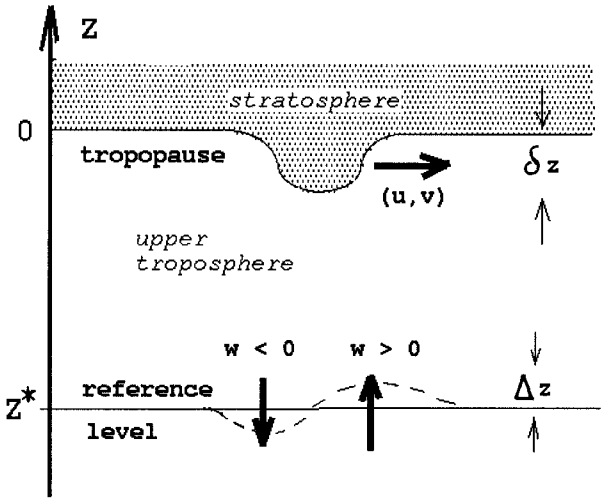

FIG. 6. Schematic illustrating the quasigeostrophic motion (u, v) of a tropopause anomaly δz and the vertical wind w induced by the motion of the tropopause anomaly at the reference level z^* below the tropopause. The reference level is supposed to be close to the isosteric surface whose temperature determines the WV channel radiance. The dashed line indicates the vertical motion of parcels initially located on the reference level.

or by the distribution of PV. Rather, in a cloud-free atmosphere without tropopause folds, the radiation received by the satellite is given, to a good approximation, by the temperature on an isosteric surface somewhat below the tropopause. Assume that the relevant isosteric surface is close to a reference level z^*, and consider the wind at this level (Fig. 6). In our model this wind differs from the wind at the tropopause level in two ways. First, the quasigeostrophic wind at the reference level is weaker than the quasigeostrophic wind at tropopause level owing to the exponential decay with $|z|$ described by Eq. (4). Second, and more important, the vertical wind induced by the quasigeostrophic motion of the tropopause anomaly vanishes identically at the tropopause but is nonzero below (and above). Therefore, the upper-tropospheric air motion is generally not parallel to the motion of the intrusion itself, and one may expect the evolving pattern of the WV image to differ qualitatively from the pattern of the displaced tropopause.

a. Induced vertical air motion in the upper troposphere

We first investigate the patterns of the induced vertical air motion in our model run, as they will turn out to be of primary importance. Figure 7 displays the vertical wind w at some reference level in the upper troposphere as obtained from Eq. (10). Initially (Fig. 7a), both tips of the strip move in a counterclockwise direction and thereby induce upward motion on their forward sides and downward motion on their rearward sides—the ''vacuum cleaner effect'' of Hoskins et al. (1985). At later times (Fig. 7b), there is additional strong down-

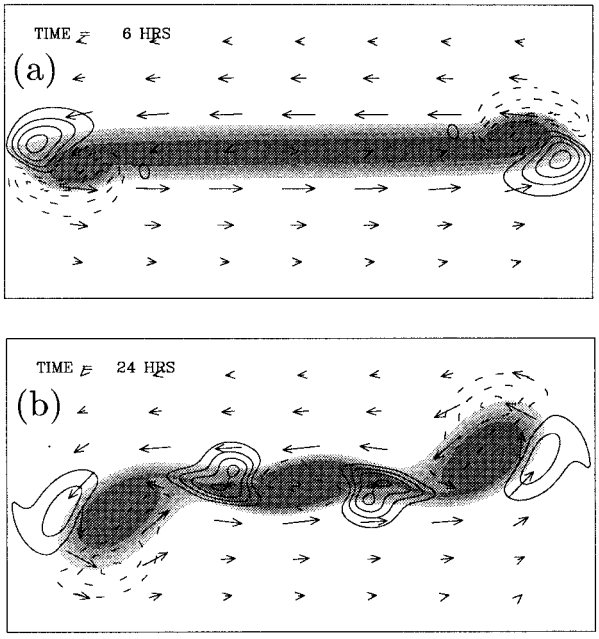

FIG. 7. Vertical velocity (cm s^{-1}) at reference level $z^* = -500$ m, (a) at $t = 6$ h, and (b) at $t = 24$ h. Contours every 0.5 cm s^{-1}, zero contour omitted; solid (dashed) contours are used for downward (upward) wind. Gray shading indicates the location of the stratospheric intrusion (cf. Fig. 5), and the arrows represent the geostrophic wind at reference level z^*.

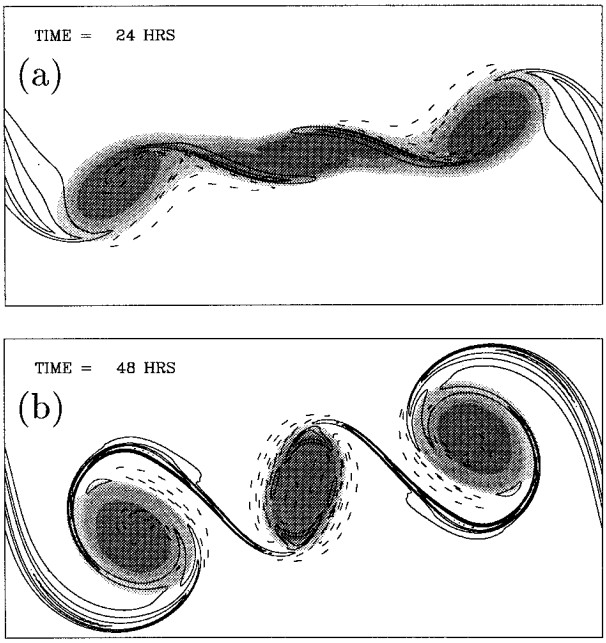

FIG. 8. Vertical displacement Δz (m) in the upper troposphere (contours every 300 m, zero contour omitted); solid contours are used for negative (downward) displacement, dashed contours for positive (upward) displacement. (a) At $t = 24$ h and (b) at $t = 48$ h. Gray shading indicates the location of the stratospheric intrusion (cf. Fig. 5).

ward motion underneath the filaments connecting the forming vortices. The reference level was chosen to be at $z^* = -500$ m. This is somewhat closer to the tropopause than suggested by empirical studies concerning the effective level of emission (some 1–2 km below the tropopause) to be in line with the model assumption of a shallow tropopause anomaly (see above).

In the current context, the vertical wind is relevant since it displaces air vertically. We consider a parcel that started at reference altitude z^* at initial time t_0, and we denote by $\Delta z(\mathbf{x}, t)$ the vertical displacement of such a parcel that has reached horizontal position $\mathbf{x}$ at time t. The evolution of Δz is given by

$$\frac{\partial \Delta z}{\partial t} + \mathbf{u}_g \cdot \nabla \Delta z = w, \tag{15}$$

where $\Delta z = 0$ is used as an initial condition and where both $\mathbf{u}_g$ and w have to be evaluated at the parcel's position. Consistent with the approximations of the QGT model made so far, we assume that $\mathbf{u}_g(x, y, z^* + \Delta z)$ and $w(x, y, z^* + \Delta z)$ in Eq. (15) can be approximated by $u_g(x, y, z^*)$ and $w(x, y, z^*)$, respectively. In other words, the wind at reference level is considered to be representative for the upper-tropospheric air motion in the neighborhood of the effective level of emission. It follows that Δz approximately behaves like a horizontally advected tracer with initial distribution $\Delta z = 0$ everywhere and with source w. Equation (15) is solved numerically making the above approximations. The horizontal advection is performed with the original time step Δt. The vertical velocity w is calculated only once every hour, when the right-hand side of Eq. (15) is accounted for by adding $w\tilde{\Delta}t$ to Δz with $\tilde{\Delta}t = 1$ h. The resulting displacement field is contoured in Fig. 8. After about 1 day of integration the upper-tropospheric vertical displacement Δz has extreme values of the order of ± 1 km giving a horizontal variation comparable to that of the tropopause displacement δz.

b. Simulation of water vapor and cloud images

We simulate WV images in our model in order to enable a qualitative comparison between the model and observed satellite images. The anomaly ΔT_{bb} of the equivalent blackbody temperature will be modeled as the sum of three contributions:

$$\Delta T_{bb} = \Delta T_{bb}^{hist}(\delta z_0) + \Delta T_{bb}^{disp}(\Delta z) + \Delta T_{bb}^{cloud}(\Delta z), \tag{16}$$

where the important parameters are the tropopause displacement at initial time $\delta z_0 \equiv \delta z(t = 0)$ and the upper-tropospheric vertical displacement Δz. The term ΔT_{bb}^{hist} represents the anomaly in specific humidity that forms previous to our initial time, $t = 0$, as the PV streamer is created by meridional advection across the background gradients (Appenzeller and Davies 1992). In the subsequent evolution, which is assumed to take place more or less at a fixed latitude, these background gradients will be neglected. The terms ΔT_{bb}^{disp} and ΔT_{bb}^{cloud}

represent changes that occur through vertical displacement during the simulated evolution of the vortex roll-up. They are set to zero initially.

At initial time, for lack of more detailed information, the anomaly in equivalent blackbody temperature $\Delta T_{bb}^{hist}(t = 0)$ is parameterized in terms of the tropopause displacement δz_0. As detailed in appendix A, empirical considerations suggest the following relation:

$$\Delta T_{bb}^{hist}(t = 0) \approx \gamma_1 \delta z_0, \tag{17}$$

with $\gamma_1 = -4$ K km^{-1}. This relation is consistent with the familiar notion that a downward displaced tropopause ($\delta z_0 < 0$) is associated with a dark (i.e., warm, $\Delta T_{bb} > 0$) feature on the WV image (cf. end of section 3a). The precise structure of ΔT_{bb}^{hist} is not important for the conclusions of this paper, but it serves to illustrate the subsequent dynamics. The pattern $\Delta T_{bb}^{hist}(x, y)$ will be horizontally advected, reflecting the horizontal advection of the initial specific humidity anomaly:

$$\frac{\partial}{\partial t}\Delta T_{bb}^{hist} = -\mathbf{u}_g(z^*)\cdot\nabla\Delta T_{bb}^{hist}. \tag{18}$$

Hence, at initial time the pattern of ΔT_{bb}^{hist} equals the pattern of the tropopause displacement δz by construction, but at later times both patterns differ to the degree that the geostrophic wind $\mathbf{u}_g$ at the reference level differs from the geostrophic wind at tropopause level. Figure 9a (cf. Fig. 5c) illustrates the point. The difference turns out to be rather small.

As shown next, the vertical wind modifies the image considerably. Equation (15) is solved for the vertical displacement $\Delta z(x, y, t)$, which, in turn, is related to a vertical shift of the effective level of emission, eventually leading to a change, ΔT_{bb}^{disp}, of the equivalent blackbody temperature. It is argued in appendix B that, to a reasonable approximation, the net effect can be parameterized as

$$\Delta T_{bb}^{disp} \approx \gamma_2 \Delta z, \tag{19}$$

with $\gamma_2 = -8.5$ K km^{-1}. Accounting for both ΔT_{bb}^{hist} and ΔT_{bb}^{disp} gives the image shown in Fig. 9b. Comparison with Fig. 9a shows significant qualitative differences. By construction, these differences in pattern can only be caused by the upper-tropospheric vertical displacement (Fig. 8).

Finally, the occurrence of clouds is accounted for using a rather simple scheme. Whenever Δz in our calculations exceeds a certain positive threshold Δz_c, we assume that high clouds form, resulting in a decrease ΔT_c of the equivalent body temperature. Thus,

$$\Delta T_{bb}^{cloud} = \Delta T_c \mathcal{H}[\Delta z(t) - \Delta z_c], \tag{20}$$

with $\mathcal{H}$ denoting the Heaviside step function [i.e., $\mathcal{H}(x) = 1$ for $x \geq 0$, $\mathcal{H}(x) = 0$ for $x < 0$]. The two parameters were chosen to be $\Delta z_c = 500$ m and $\Delta T_c = -5$ K, yielding a modification that is minor, albeit detectable (Fig. 9c). In our model run, the effect of the clouds is mostly seen as a reinforcement of the white patches in the center of the two outer vortices.

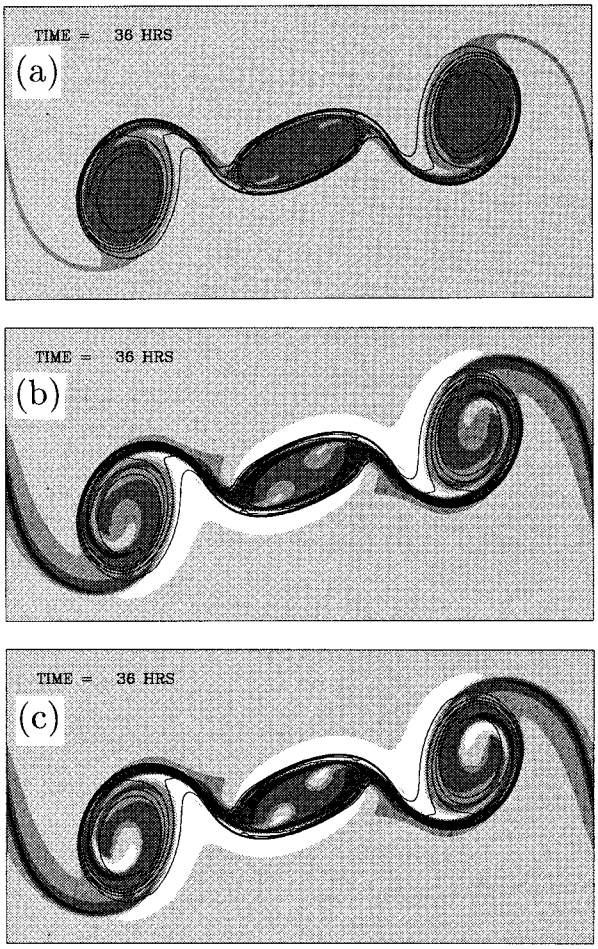

FIG. 9. Simulated equivalent blackbody temperature T_{bb} (gray shading) as seen by the WV channel of a satellite. More precisely [cf. Eq. (16)], the shading gives the perturbation of ΔT_{bb} according to (a) $\Delta T_{bb} = \Delta T_{bb}^{hist}$, i.e., a hypothetical case of no vertical motion in the upper troposphere; (b) $\Delta T_{bb} = \Delta T_{bb}^{hist} + \Delta T_{bb}^{disp}$, i.e., accounting for the effect of upper tropospheric vertical motion; (c) $\Delta T_{bb} = \Delta T_{bb}^{hist} + \Delta T_{bb}^{disp} + \Delta T_{bb}^{cloud}$, i.e., as in (b) but adding a simple parameterization of the effect of clouds. The steps in the gray tones are every 5 K, and dark (light) shading stands for positive (negative) ΔT_{bb}. The location of the stratospheric intrusion is indicated by the solid contours (cf. Fig. 5).

The two constants γ_1 and γ_2 quantify the relative importance of $\delta z(t = 0)$ and $\Delta z(t)$ for affecting the WV channel radiance. As $|\gamma_2||\gamma_1|^{-1} \approx 2$, the impact of a parcel's vertical displacement Δz during the course of the evolution is about twice as big as an initial tropopause displacement δz_0 of the same size. While at initial time there is only an effect related to tropopause displacement, at later times the effect of the subsequent vertical air displacement dominates as soon as typical values of Δz have reached the same magnitude as typical values of δz. Note that if the atmosphere was characterized by homogeneous relative humidity at initial time,

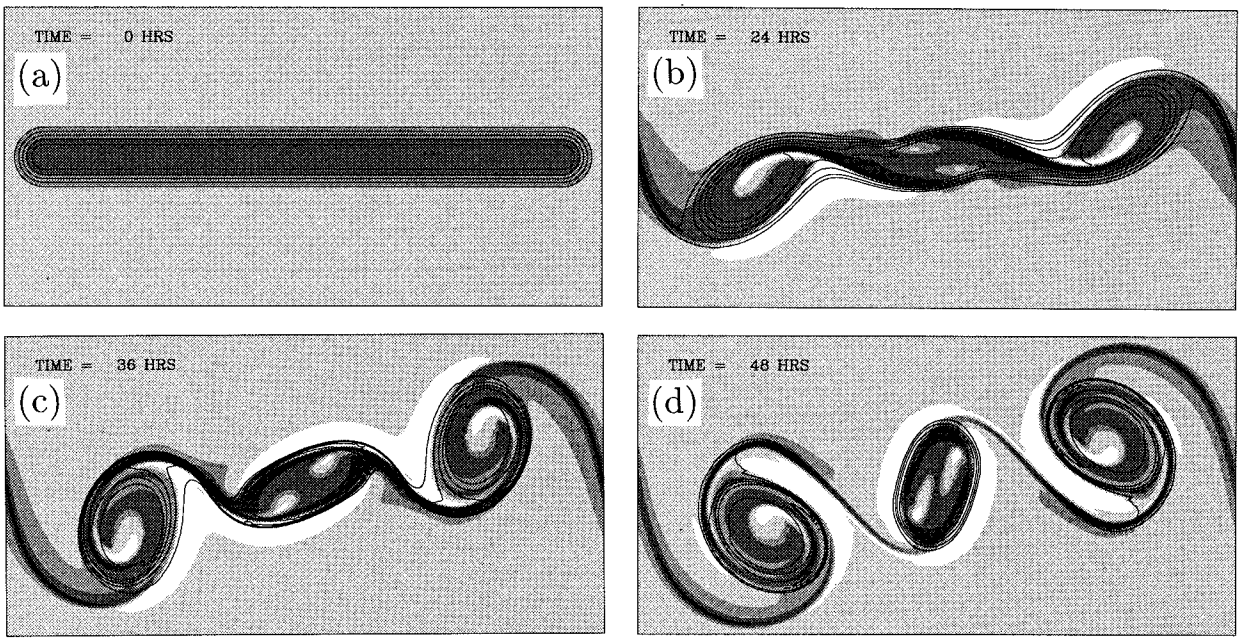

FIG. 10. Simulated equivalent blackbody temperature T_{bb} (gray shading) as seen by the WV channel of a satellite (a) initially, (b) at t = 24 h, (c) at t = 36 h, and (d) at t = 48 h. More precisely, the shading gives the perturbation of ΔT_{bb} according to Eq. (16) with the steps in the gray tone every 5 K; dark (light) shading stands for positive (negative) ΔT_{bb}. The location of the stratospheric intrusion is indicated by the solid contours (cf. Fig. 5).

one would expect to see hardly any signature of the downward tropopause displacement in spite of the low tropopause and the low absolute humidity in the cold anomaly (Möller 1961; Soden and Bretherton 1993). The fact that a stratospheric streamer is visible on real WV images even before it starts to roll up indicates that there is likely to have existed some downward motion during its formation through meridional advection. In this sense the contribution ΔT_{bb}^{hist} in (16) can be considered as a rough parameterization of the integrated effect of the vertical motions that have taken place before time $t = 0$.

Figure 10 illustrates the evolution of ΔT_{bb} for the current run. Comparison of the equivalent blackbody temperature (shading) with the corresponding tropopause displacement (contours; see also Fig. 5) reveals considerable qualitative differences. Overall, there is more detailed structure in the simulated WV images than on the plots of the tropopause displacement. In particular, there is considerable structure on the WV image in the center of the vortices, while the tropopause displacement is quite homogeneous there. In addition, the dark filaments appear stronger in the WV image than on the tropopause map, and their appearance is reinforced by the presence of white filaments that do not exist on the tropopause map. As a result, the simulated WV image has a rather spiral-like appearance—a feature commonly observed on WV images.

Our simple parameterization of cloud formation yields the evolution of the cloud pattern as shown in Fig. 11. Not surprisingly, clouds appear in locations where the WV image is white (indicating high humidity), since both are caused by upward vertical air motion. On the other hand, dark features are absent on the cloud image. This qualitative difference between our WV images and our cloud images is in good agreement with observations (see Fig. 2).

In the above model run the reference level was chosen to be at $z^* = -500$ m. To illustrate the sensitivity of T_{bb} with respect to z^*, the above run is reanalyzed for a reference level at $z^* = -1$ km, that is, more distant from the tropopause than before (Fig. 12). Now the larger horizontal scales are more dominant, since the horizontal and vertical scales are intrinsically related in Juckes's model [see Eq. (4)]. Also, the evolution is somewhat slower than before owing to the exponential decay with $|z|$ of the geostrophic streamfunction. The qualitative features, however, are similar as in the previous run and, correspondingly, the main conclusions of our paper are not affected by the particular value of z^*. Similarly, the differences between the model WV and tropopause maps turned out to be very robust with respect to the specific choice of the initial state. For a range of different initial states tried, the simulated WV image always displayed considerably more detailed structure than the tropopause displacement in the sense described above. In particular, these results did not depend sensitively on the steepness of the gradients in the initial intrusions. Note, incidentally, that the ''detailed structures'' on the simulated WV images are not really very small scale and that they would not disappear if viewed with somewhat lower resolution.

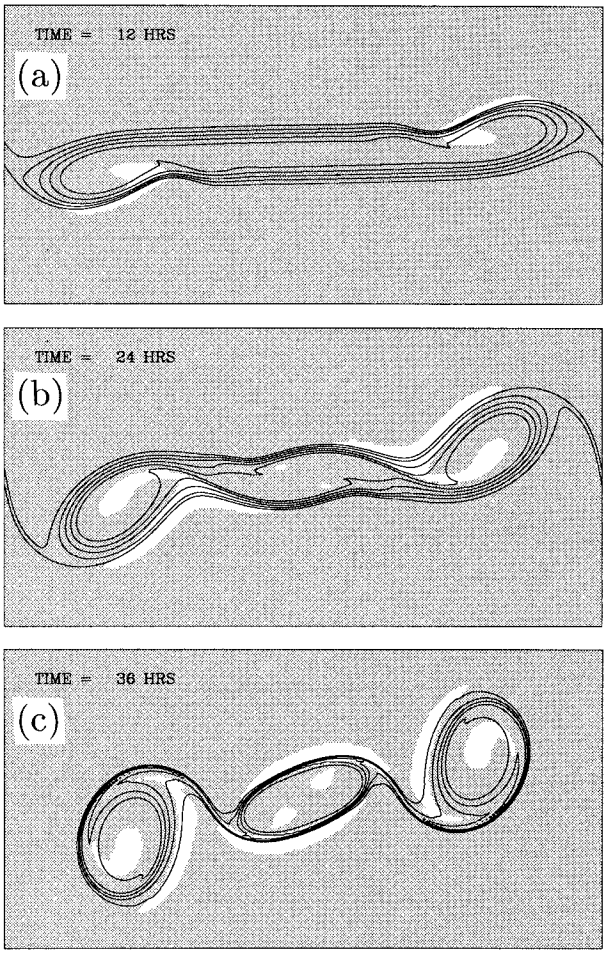

FIG. 11. Simulated cloud pattern at (a) $t = 12$ h, (b) $t = 24$ h, and (c) $t = 36$ h. Areas where clouds have formed are white, while cloud-free areas are gray. The contours indicate the location of the stratospheric intrusion (cf. Fig. 5).

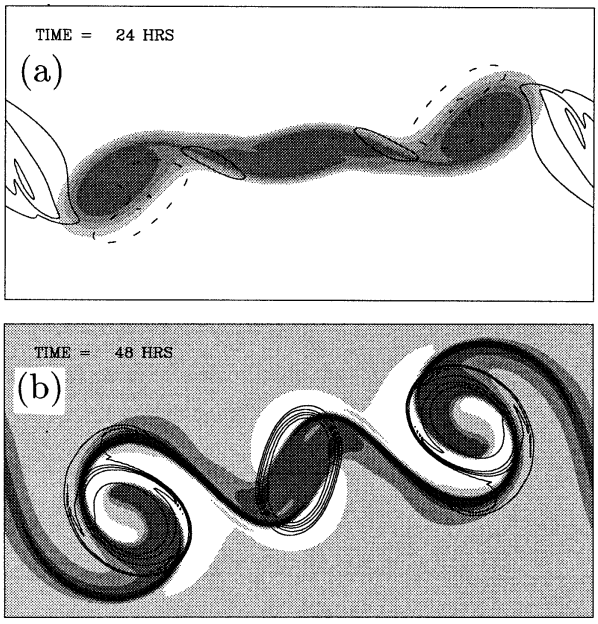

FIG. 12. Same model run and plot type as in Figs. 8 and 10, respectively, except that here the reference level is located at $z^* = -1000$ m instead of $z^* = -500$ m. (a) Vertical displacement Δz at $t = 24$ h (to be compared with Fig. 8a) and (b) equivalent blackbody temperature at $t = 48$ h (to be compared with Fig. 10d).

The variation of horizontal advection with altitude may result in a vertical tilt of the filaments in the moisture distribution during the course of the evolution (e.g., Figs. 10d vs 12b). This could lead to moist air locally overlying the dry filament, which may explain why on observed WV images the dark filaments often disappear after some time. This effect of the vertical tilt, however, is not accounted for in our method for generating bogus WV images.

c. Mechanistic interpretation

As apparent from Fig. 7, a preferred region for rising motion is the leading edge of the streamer, which turns counterclockwise and which is about to roll up. It was mentioned before that this is the so-called vacuum cleaner effect: upward motion is forced when an upper-air PV anomaly approaches overhead (cf. Fig. 6). Part of the air that is displaced upward is subsequently drawn right underneath the vortex by the horizontal advection (Fig. 8a) such that the WV image appears white rather than dark (Figs. 10b–d). This part of the air becomes trapped in the center of the vortex and does not flow through to the region of descent. The upward displacement indicated by the white patch therefore becomes a semipermanent feature. Note that these patches are located in areas on the WV image where one might have expected it to be dark from considerations of the tropopause displacement alone. Another part of the air that is displaced upward undergoes strong horizontal stretching resulting in long white filaments right next to the dark filament connecting the isolated vortices. As a consequence, there is an intermingling of dark and light filaments, which gives the WV image a typical spiral-like appearance.

Similarly, one can give a mechanistic explanation of the strong downward forcing underneath the dark filaments connecting the vortices. These filaments are generated during the fragmentation as certain parts of the high-PV stratospheric air move apart, tending to concentrate in isolated blobs of PV. Recall that the vertical displacement (upward) of upper tropospheric isentropes is opposite to the displacement (downward) of the tropopause (see Fig. 4). At the initial time, the anomaly in the height of the isentropes actually reflects their equilibrium height at more poleward latitudes, from which the streamer was advected. Since the streamer is stretched out into an extremely narrow band between the forming vortices, and since the smallest horizontal scales are not represented some distance below the tropopause [see Eq. (4)], the upper-troposopheric isentro-

pes right in between forming vortices move downward, approaching the equilibrium altitude corresponding to the current latitude. In the current run the maximum downward wind occurs right underneath the dark filament, connecting the inner vortex with the outer two vortices at time $t = 30$ h, that is, at the time when the process of separation of the vortices is most intense (cf. Fig. 7b). The forced downward motion leads to drying and, therefore, to a significant enhancement of the connecting filaments in the WV image, where they now appear as distinct dark bands (Fig. 10)—much darker than one would expect from the thin filaments of the stratospheric intrusion alone (Fig. 5). In addition, this effect creates new dark filaments connecting the outer two vortices (remember: doubly periodic boundary conditions), which are practically nonexistent on the tropopause map. Note that in Fig. 10d the dark bands connecting the middle vortex with the two adjacent vortices are on the verge of disappearing due to numerical diffusion.

All the features discussed above—the existence of white patches in the center of the rolling-up vortices, the strength and the thickness of the connecting filaments and the existence of white filaments right next to the dark filaments—are observed on WV images (e.g. Fig. 2a). Thus, even though the model is too idealized to allow a quantitative comparison with observations, it is able to reproduce many of the essential structural elements of observed WV images in a qualitatively correct way.

Finally, we note that Eq. (15), which describes the vertical displacement of a material surface being relevant for the simulation of the WV image, is isomorphic with the near-surface relative vorticity equation, if in the latter the stretching term $f\partial w/\partial z$ is approximated by $fw(z^*)/z^*$ and if the relative vorticity ζ is identified with $f\Delta z/z^*$. The upper-tropospheric horizontal and vertical air motions affect, therefore, relative vorticity and the WV image in a similar manner so that the former could also be taken as a qualitative proxy for the latter. The expected similarity shows well in our current model runs, as can be seen through a comparison of our model-generated WV images with Fig. 13, where we show relative vorticity at $z = 0$. This equivalence also explains why structures seen on WV images resemble those seen in vorticity in simulations of surface frontal instability (Schär and Davies 1990).

d. Experiment with a ''passive tropopause''

The analysis so far has clearly shown that the increased amount of spiral-like structures in our model-generated WV images can be attributed to the impact of the vertical wind on upper-tropospheric moisture. To the degree that the model correctly represents the qualitative nature of the key processes involved, these processes can be assumed to be operating in the real atmosphere, too. However, we must first explain a discrepancy between our model results and the results from various other studies (e.g., Bush and Peltier 1994; Appenzeller et al. 1996; Bithell et al. 1997, manuscript submitted to *J. Atmos. Sci.*). In these studies more realistic models than our current one were used. In contrast to our results, they generally obtained a great deal of spiral-like structures on their PV or tropopause maps, and the vortex core was not always characterized by a homogeneous distribution of high PV or low tropopause displacement.

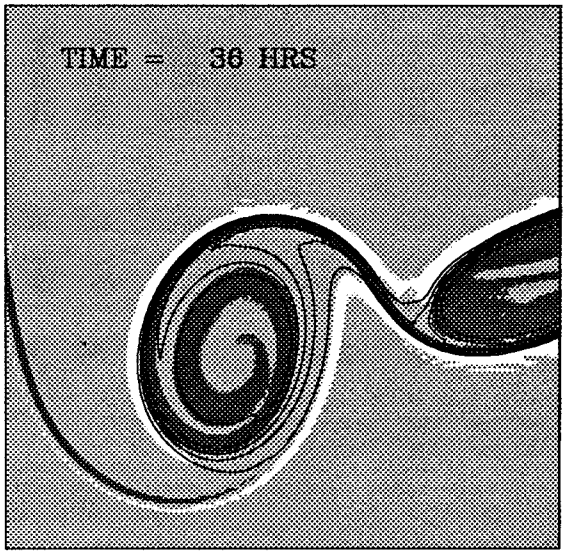

FIG. 13. Relative vorticity at $z = 0$ at time $t = 36$ h. The dark and light shading denotes areas where the relative vorticity is greater than $2f$ and less than $-2f$, respectively. The contours indicate the location of the stratospheric intrusion (cf. Fig. 5).

We suggest the following explanation. In the case of a sizeable intrusion like the one shown in Fig. 3, stratospheric air with PV values of 6–8 PVU descends below the level of the unperturbed tropopause. To the degree that the dynamics of this anomaly are predominantly quasi-two-dimensional, the PV is expected to concentrate in isolated, almost axisymmetric, vortices with rather sharp horizontal PV gradients at the vortex edge and a fairly homogeneous vortex core (McWilliams 1984; Melander et al. 1987; Legras and Dritchel 1993). Such a qualitative behavior is indeed supported by the isentropic contour advection calculations of Appenzeller et al. (1996), in which the spiraling structures are rather pronounced at lower values of potential temperature but give way to a more uniform vortex core at higher values of potential temperature. This suggests that the overall dynamics is effectively driven by the high-PV interior of the intrusion. On the other hand, a material surface corresponding to a lower PV value is advected more like a passive tracer, very much like the filaments outside the edge of the stratospheric polar vortex are advected quasi-passively in the wind field, which is predominantly determined by the strong polar vortex itself (McIntyre and Palmer 1984; for related studies see also

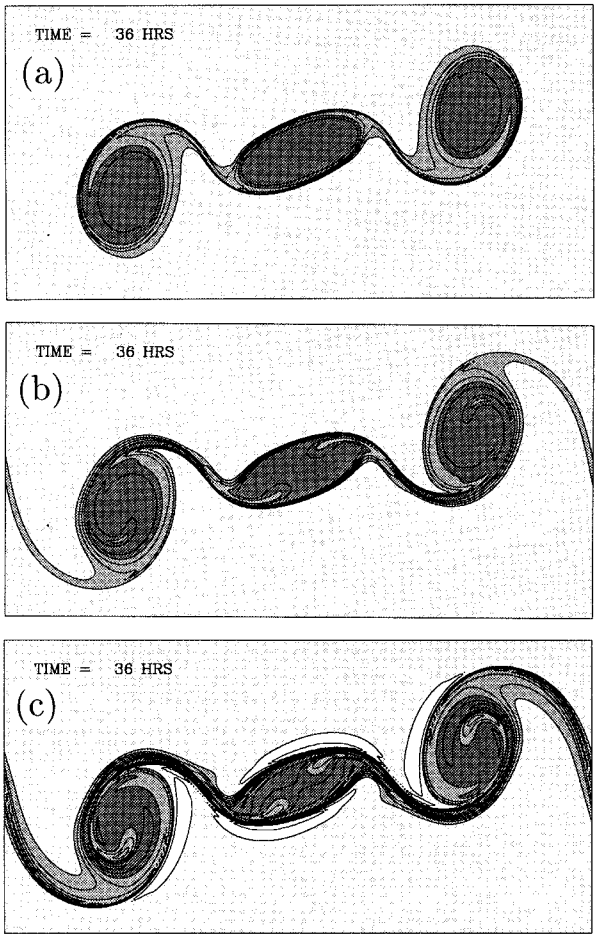

FIG. 14. Model experiment with a ''passive tropopause.'' The plot (both contours and shading) shows the displacement of a material surface at time $t = 36$ h, which has been initialized at time $t = 0$ with the tropopause displacement δz and which has been advected (a) horizontally with (u_g, v_g, 0) at $z = 0$, (b) horizontally with (u_g, v_g, 0) at $z = z^*$, and (c) both horizontally and vertically with (u_g, v_g, w_a) at $z = z^*$, with $z^* = -500$ m. Contours every 500 m with the zero contour omitted. Dark (light) shading indicates downward (upward) displacement.

Babiano et al. 1987; Dritchel 1989; Dritchel et al. 1991). Because in the current model the PV anomaly is effectively concentrated in an infinitely shallow layer [Eq. (14)], its evolution is likely to be representative for the evolution of the dynamically dominant high PV interior of the incipient vortex. This would explain why on our tropopause maps there tends to be little to no spiral structure within the vortex core. Studies with more realistic models, on the other hand, tend to define the location of the tropopause through a fairly low value of PV—typically PV = 2 PVU, but sometimes even as low as PV = 1 PVU (Bush and Peltier 1994; Bithell et al. 1997, manuscript submitted to *J. Atmos. Sci.*). Using T42 ECMWF analyses, Grewe and Dameris (1995), for instance, showed that in the zonal mean the 1- and 2-PVU surfaces at northern midlatitudes are approximately located at 450 and 350 hPa, respectively. This is significantly below the WMO-defined thermal tropopause, which typically coincides with PV = 3.5 PVU. The appearance of a great deal of finescale structures could be attributed to the choice of a fairly low PV value.

The relevance of the above argument can be tested in the current context through an additional simple experiment with our model. In this experiment we consider the advection of a quasi-horizontal material surface that initially has precisely the structure of the tropopause except for a uniform downward displacement by z^*. This surface is interpreted as the analog in our QGT model of the tropopause in more realistic models, if the latter is defined through a fairly low PV value. It is referred to as the ''passive tropopause'' in the following. The wind at the passive tropopause is approximated by the wind at the reference level z^*. If the wind at reference level were identical to the wind at $z = 0$, the material surface would evolve precisely as the tropopause displacement itself (Fig. 14a). When one accounts for the difference in the horizontal wind between the level $z = 0$ and $z = z^*$, but still neglects the effect of the vertical wind, one obtains a somewhat modified evolution owing to the exponential decay with $|z|$ of the geostrophic wind (Fig. 14b). As expected, it is primarily the impact of the vertical wind at a reference level that leads to a much enhanced structure of the passive tropopause in comparison with the structure of the actual model tropopause (Fig. 14c). Note that, by construction, the pattern of the passive tropopause is qualitatively similar to that of the simulated WV image in Fig. 10. The difference between the two lies mostly in the factor of $|\gamma_2||\gamma_1|^{-1} \approx 2$, which amplifies the relative contribution of the vertical wind in the latter case.

The above experiment with the passive tropopause shows that caution is needed when talking about ''the'' tropopause, as this implicitly assumes a single uniquely defined surface. Both in the real atmosphere and in realistic models there is a continuous (albeit often thin) transition zone between the troposphere and the stratosphere. Depending on the precise definition of the tropopause, that is, whether it is located more at the periphery of the stratospheric intrusion or more toward the core of the intrusion, one may obtain quite different structures during the course of its evolution. To the degree that the tropopause is defined through a fairly low value of PV (compared with PV values in the interior of the intrusion), and even more so to the degree that the isosteric surface relevant for the WV image is located somewhat below the tropopause, one expects both to feature a considerable amount of spiraling structures, even though the interior of the intrusion is likely to roll up into a more solid core as suggested by the evolution of our idealized quasigeostrophic tropopause.

5. Summary and conclusions

In the current paper we investigated in some detail the quasi-horizontal roll-up of fragmenting stratospheric

intrusions, how the structures seen on WV images are actually generated, and how they are related to those seen on maps of the tropopause height or on maps of PV. We explicitly accounted for the fact that a WV image does not really give an image of the tropopause intrusion, adopting the approach of Ramond et al. (1981), according to whom the WV channel radiance is approximately proportional to the temperature on an upper-tropospheric isosteric surface.

An idealized model for quasigeostrophic tropopause dynamics (Juckes 1994) was used to obtain a high-resolution (in the horizontal) integration of the roll-up of a fragmenting stratospheric intrusion. As an initial condition, a V-shaped strip of stratospheric air embedded in the upper troposphere was specified. The strip breaks up and the high-PV stratospheric air concentrates in a number of isolated vortices, which are characterized by rather uniform cores and which are connected by thin filaments. We explicitly calculated the vertical wind and we derived an approximate measure for the vertical displacement of air parcels in the upper troposphere. Then we simulated the combined effect of the initial tropopause displacement, induced upper-tropospheric displacement, and clouds induced by the vertical wind on the equivalent blackbody temperature seen by the WV channel of a satellite. Consistent with observations, an initial downward tropopause displacement was assumed to be related to a dark feature on the WV image. During the course of the evolution the induced vertical wind substantially modifies this picture. It was shown that a material surface (passive tropopause), which is located somewhat below the dynamically active model tropopause, acquires considerably more spiraling structures than the more compact model tropopause. The height of such passive tropopause, in turn, is approximately related to the temperature on an upper-tropospheric isosteric surface. Therefore, it is plausible that the structures on our simulated WV images closely resembled the structures of the passive tropopause, both being much richer in structure than the actual model tropopause. Furthermore, because the equation for the evolution of the passive tropopause is approximately isomorphic to the equation for the near-tropopause relative vorticity, the pattern of relative vorticity is qualitatively closer to the pattern of the WV images than to the pattern of the tropopause displacement or the tropopause potential temperature. These results turned out to be robust with respect to the specific choice of the initial condition.

The qualitative differences in our model between the patterns of the tropopause height and the simulated WV image were explained mechanistically. There is forcing of upward motion underneath the leading edge of the intrusion as it is about to roll up horizontally. Part of the air that has undergone upward forcing is subsequently drawn into the vortex center right under the depressed tropopause, which therefore appears lighter than one might have anticipated from consideration of the tropopause displacement alone. Another part of the air that has undergone upward forcing is stretched out into thin white filaments and is advected right next to the dark filaments that connect the isolated vortices. On the other hand, the air between the forming vortices experiences strong downward forcing, which reinforces existing dark filaments on the WV image and creates new ones. All these simulated features are commonly observed on actual WV images. Regarding the robustness of our results and the fairly basic mechanistic interpretation that we were able to provide, we believe that our study has qualitative relevance to the real atmosphere despite the simplicity of the model used.

In more realistic models or in the real atmosphere the dynamics are dominated by the high-PV interior of the intrusion. On the other hand, the tropopause is often defined through a fairly low value of PV. As a consequence, the tropopause is advected almost like a passive tracer and is subject to induced vertical motions similarly to an upper-tropospheric isosteric surface. This may plausibly result in structures of ''the tropopause'' that are quite similar to the structures on the WV image. By contrast, the tropopause in our idealized model probably reflects the dynamically dominant core part of the intrusion; the latter is expected to behave qualitatively like two-dimensional and geostrophic flows in the sense of yielding little structure in the vortex interior.

We conclude that a substantial portion of the spiral-like structures on WV images showing the roll-up of a fragmenting stratospheric intrusion is likely to reflect the vertical wind induced by the evolution of the intrusion itself. When the tropopause is defined through a fairly low value of PV, it may acquire similar spiraling structures, as it is being advected almost like a passive tracer. On the other hand, for the dynamically active core part of the intrusion, which is located above the tropopause, one may expect an evolution leading to more compact vortex cores and overall less structure.

Acknowledgments. We would like to thank two anonymous referees for helpful comments and our colleagues for useful discussions.

APPENDIX A

Relation between Tropopause Displacement and Equivalent Blackbody Temperature at Initial Time

The initial state representing a stratospheric intrusion implicitly contains the complex history of its formation. We chose a quasi-empirical approach for the simulation of the initial equivalent blackbody temperature anomaly $\Delta T_{\mathrm{bb}}^{\mathrm{init}} \equiv \Delta T_{\mathrm{bb}}^{\mathrm{hist}}(t = 0)$. As discussed in connection with Fig. 3, at initial time the tropopause displacement δz should be a fairly good estimate for the displacement of the relevant isosteric surface. Furthermore, it is assumed that the isosteric surface is close enough to the tropopause so that its initial temperature perturbation

ΔT_{bb}^{init} can be approximated by the temperature perturbation $\Delta T|_{\delta z}$ on the displaced tropopause.

The temperature perturbation $\Delta T|_{\delta z}$, in turn, can be obtained as follows. Assuming that $p \approx p_0 \exp(-z/H)$ with constants p_0 and H, the temperature is given by $T = \theta(p/p_0)^{\kappa} \approx \theta \exp(-\kappa z/H) = T[\theta(z), z]$ with $\kappa = 2/7$. In the presence of a temperature perturbation, $\theta'(x, y, z)$, the temperature anomaly $\Delta T(x, y)$ on a material, quasi-horizontal surface, which is locally displaced by $\delta z(x, y)$, is given by

$$\Delta T(\theta', \delta z) \approx \left.\frac{\partial T}{\partial \theta}\right|_{\delta z=0} \theta' + \left.\frac{\partial T}{\partial z}\right|_{\theta'=0} \delta z. \qquad \text{(A1)}$$

The value of $\partial T/\partial\theta = (p/p_0)^{\kappa}$ is about 2/3 for $p_0 = 1000$ hPa and the tropopause at $p \approx 200$ hPa. Within the framework of Juckes's model the temperature perturbation at some constant z below, but close to the tropopause, is given by $\theta' = N_s^{-1}(N_s - N_t)\theta'_{tp}$, which follows from (4), (5), and (8). Thus, using the values for N_s and N_t given in section 3c, the first term on the right-hand side of (A1) reduces to $\frac{2}{3}\theta' = \frac{2}{3}(\theta'_{tp}/2) = \theta'_{tp}/3$. The lapse rate $\partial T/\partial z = T_z$ is given in terms of potential temperature as $T_z = (\partial\theta/\partial z - \kappa\theta/H)(p/p_0)^{\kappa}$, which in the upper troposphere yields $T_z \approx -6$ K km^{-1}. Using Eq. (2), the right-hand side of (A1) can be written as $\frac{1}{3}\theta'_{tp} + T_z\delta z$.

Putting the above together yields

$$\Delta T_{bb}^{init} \approx \Delta T|_{\delta z} \approx \frac{1}{3}\theta'_{tp} + T_z\delta z = \left(\frac{1}{3}\frac{\theta_{oo}}{g}N_tN_s + T_z\right)\delta z \qquad \text{(A2)}$$

$$= \left(\frac{6}{3}\ \text{K km}^{-1} - 6\ \text{K km}^{-1}\right)\delta z = -4\ \text{K km}^{-1}\delta z. \qquad \text{(A3)}$$

The coefficient $\gamma_1 = -4$ K km^{-1}, relating δz and ΔT_{bb}^{init}, is smaller than a typical upper-tropospheric lapse rate, since the (cold) temperature anomaly underneath a lowered tropopause partly compensates for the increase in temperature with decreasing altitude. (See Fig. 4, where the compensation appears as an upward bulging of the isentropes underneath the tropopause intrusion. An indication of this ''compensation'' can be found in the observed section in Fig. 3, where the isotherms are slightly displaced downward underneath the intrusion.)

APPENDIX B

Change in Equivalent Blackbody Temperature Induced by Subsequent Vertical Air Displacement

Consider an air parcel that originally was located somewhat below the tropopause at the effective level of emission and that is subsequently displaced vertically by the amount Δz. Assuming an unsaturated atmosphere, the parcel experiences a temperature change of $\Delta T = \Gamma_d\Delta z$, with the dry adiabatic lapse rate $\Gamma_d \approx -10$ K km^{-1}. If the effective level of emission was given by a surface of constant water vapor mixing ratio, s, then the change of equivalent blackbody temperature would be given by

$$\Delta T_{bb}|_{\Delta z}\ (\text{on } s = \text{const}) = \Gamma_d\Delta z, \qquad \text{(B1)}$$

since s is materially conserved. However, the effective level of emission is not really given by an isopleth of specific humidity (s = const), but according to Ramond et al. (1981) to a good approximation by an isosteric surface ($\rho_w = s\rho$ = const). As opposed to s, the density of water vapor ρ_w is not materially conserved upon vertical displacement; owing to the parcel's change in density ρ, the effective level of emission is displaced by less than Δz. This effect is accounted for as follows. Assuming exponential profiles for ρ and s with constant scale heights H_ρ and H_s, respectively, the constraint $\Delta(s\rho) = 0$ for a point on an isosteric surface leads to

$$\frac{\Delta s}{s} \equiv \frac{-\Delta z'}{H_s} = -\frac{\Delta\rho}{\rho} \equiv \frac{\Delta z}{H_\rho}, \qquad \text{(B2)}$$

where $\Delta z'$ denotes the vertical shift of the effective level of emission with respect to the parcel's displaced position, which is necessary in order to satisfy the constraint. It follows that $\Delta z' = -(H_s/H_\rho)\Delta z \approx -\Delta z/4$ for $H_\rho \approx 8000$ m and $H_s \approx 2000$ m. Neglecting the (small) change in lapse rate T_z due to the vertical displacement, the altitude difference $\Delta z'$ between the new parcel position and the new position of the isosteric level implies a ''correction'' of ΔT by the amount $T_z\Delta z'$. Hence, the change in equivalent blackbody temperature due to vertical air motion is approximated by

$$\Delta T_{bb}|_{\Delta z} \approx \Gamma_d\Delta z + T_z\Delta z' \approx \left(\Gamma_d - \frac{T_z}{4}\right)\Delta z. \qquad \text{(B3)}$$

With the values for Γ_d and T_z used before this yields

$$\Delta T_{bb}|_{\Delta z} \approx \left[-10\ \text{K km}^{-1} - \frac{(-6)}{4}\ \text{K km}^{-1}\right]\Delta z = -8.5\ \text{K km}^{-1}\Delta z. \qquad \text{(B4)}$$

The coefficient $\gamma_2 = -8.5$ K km^{-1}, relating Δz and

$\Delta T_{bb}|_{\Delta z}$, is close to the dry adiabatic lapse rate Γ_d. As a consequence the temperature anomaly on an isosteric surface deviates only slightly from the temperature anomaly on a surface of constant water vapor ratio [cf. (B1) with (B3)].

REFERENCES

Appenzeller, C., and H. C. Davies, 1992: Structure of stratospheric intrusions into the troposphere. *Nature,* **358,** 570–572.

——, ——, and W. A. Norton, 1996: Fragmentation of stratospheric intrusions. *J. Geophys. Res.,* **101,** 1435–1456.

Babiano, A., C. Basdevant, B. Legras, and R. Sadourny, 1987: Vorticity and passive-scalar dynamics in two-dimensional turbulence. *J. Fluid Mech.,* **183,** 379–397.

Bretherton, F. P., 1966: Critical layer instability in baroclinic flows. *Quart. J. Roy. Meteor. Soc.,* **92,** 325–334.

Browning, K. A., 1993: Evolution of a mesoscale upper tropospheric vorticity maximum and comma cloud from a cloud-free two-dimensional potential vorticity anomaly. *Quart. J. Roy. Meteor. Soc.,* **119,** 883–906.

——, and N. M. Roberts, 1994: Use of satellite imagery to diagnose events leading to frontal thunderstorms: Part I of a case study. *Meteor. Appl.,* **1,** 303–310.

——, and ——, 1995: Use of satellite imagery to diagnose events leading to frontal thunderstorms: Part II of a case study. *Meteor. Appl.,* **2,** 3–9.

Bush, A. B. G., and W. R. Peltier, 1994: Tropopause folds and synoptic-scale baroclinic wave life cycles. *J. Atmos. Sci.,* **51,** 1581–1604.

Dritchel, D. G., 1989: On the stabilization of a two-dimensional vortex strip by adverse shear. *J. Fluid Mech.,* **206,** 193–221.

——, P. H. Haynes, M. N. Juckes, and T. G. Shepherd, 1991: The stability of a two-dimensional vorticity filament under uniform strain. *J. Fluid Mech.,* **230,** 647–665.

Fischer, H., N. Eigenwillig, and H. Müller, 1981: Information content of METEOSAT and Nimbus/THIR water vapor channel data: Altitude association of observed phenomena. *J. Appl. Meteor.,* **20,** 1344–1352.

Grewe, V., and M. Dameris, 1995: Calculating the global mass exchange between stratosphere and troposphere. *Ann. Geophys.,* **14,** 431–442.

Held, I. M., R. T. Pierrehumbert, S. T. Garner, and K. L. Swanson, 1995: Surface quasi-geostrophic dynamics. *J. Fluid Mech.,* **282,** 1–20.

Honvault, C., 1990: The European METEOSAT. *Weather Satellites: Systems, Data, and Environmental Applications,* P. K. Rao, S. J. Holmes, L. K. Anderson, J. S. Winston, and P. Lehr, Eds., Amer. Meteor. Soc., 69–76.

Hoskins, B. J., M. E. McIntyre, and A. W. Robertson, 1985: On the use and significance of isentropic potential vorticity maps. *Quart. J. Roy. Meteor. Soc.,* **111,** 877–946.

Juckes, M., 1994: Quasigeostrophic dynamics of the tropopause. *J. Atmos. Sci.,* **51,** 2756–2768.

——, 1995: Instability of surface and upper-tropospheric shear lines. *J. Atmos. Sci.,* **52,** 3247–3262.

Legras, B., and D. Dritchel, 1993: Vortex stripping and the generation of high vorticity gradients in two-dimensional flows. *Appl. Sci. Res.,* **51,** 445–455.

Manney, G. L., and J. L. Stanford, 1987: On the relation of 6.7-μm water vapour features to isentropic distributions of potential vorticity. *Quart. J. Roy. Meteor. Soc.,* **113,** 1048–1057.

McIntyre, M. E., and T. N. Palmer, 1984: The 'surf zone' in the stratosphere. *J. Atmos. Terr. Phys.,* **46,** 825–849.

McWilliams, J. C., 1984: The emergence of isolated coherent vortices in turbulent flow. *J. Fluid Mech.,* **146,** 21–43.

Melander, M. V., J. D. McWilliams, and N. J. Zabusky, 1987: Axisymmetrization and vorticity-gradient intensification of an isolated two-dimensional vortex through filamentation. *J. Fluid Mech.,* **178,** 137–159.

Möller, F., 1961: Atmospheric water vapor measurements at 6–7 microns from a satellite. *Planet. Space Sci.,* **5,** 202–206.

Poc, M. M., M. Roulleau, N. A. Scott, and A. Chedin, 1980: Quantitative studies of METEOSAT water-vapor channel data. *J. Appl. Meteor.,* **19,** 868–876.

Ramond, D., H. Corbin, M. Desbois, G. Szejwach, and P. Waldteufel, 1981: The dynamics of polar jet streams as depicted by the METEOSAT WV channel radiance field. *Mon. Wea. Rev.,* **109,** 2164–2176.

Schär, Ch., and H. C. Davies, 1990: An instability of mature cold fronts. *J. Atmos. Sci.,* **47,** 929–950.

Shapiro, M. A., and E. D. Grell, 1994: In search of synoptic/dynamic conceptualizations of the life cycles of fronts, jet streams, and the tropopause. *Proc. Int. Symp. on the Life Cycles of Extratropical Cyclones,* Vol. I, Bergen, Norway, University of Bergen, 163–181.

Soden, B. J., and F. P. Bretherton, 1993: Upper tropospheric relative humidity from the GOES 6.7 μm channel: Method and climatology for July 1987. *J. Geophys. Res.,* **98,** 16 669–16 688.

Wirth, V., 1996: Quasi-geostrophic dynamics of an upper tropospheric PV anomaly in two idealized high resolution models and related stratosphere–troposphere exchange. *Contrib. Atmos. Phys.,* **69,** 333–347.